Deep learning-based morphology classification of activated sludge flocs in wastewater treatment plants

Hisashi Satoh[a,*], *Yukari Kashimoto*[a], *Naoki Takahashi*[b], *Takashi Tsujimura*[b]

[a]Division of Environmental Engineering, Faculty of Engineering, Hokkaido University, North-13, West-8, Sapporo 060-8628, Japan

[b]Plugin Co., Ltd., South-1, West-11, Sapporo 060-0061, Japan

E-mail addresses:

Hisashi Satoh – qsatoh@eng.hokudai.ac.jp

Yukari Kashimoto – y.kashimoto@frontier.hokudai.ac.jp

Naoki Takahashi – n.takahashi@plugins.co.jp

Takashi Tsujimura – techguy@plugins.co.jp

*Corresponding Author

Hisashi Satoh, Division of Environmental Engineering, Faculty of Engineering, Hokkaido University, North-13, West-8, Sapporo 060-8628, Japan

Tel: +81-(0)11-706-6277; Fax: +81-(0)11-706-6277; E-mail: qsatoh@eng.hokudai.ac.jp

ABSTRACT

Microscopy inspection of the morphology of activated sludge (AS) flocs can provide important information regarding the AS properties, which strongly affect the performance of AS systems. However, the acquisition of such information from microscopy inspection results requires skilled and specialized expertise. In this study, we aimed to develop two deep learning-based two-label classifiers for recognizing aggregated or dispersed flocs (Classifier-1) and the presence or absence of filamentous bacteria (Classifier-2). To achieve this, we used a convolutional neural network (CNN)-based method and selected the pre-trained Inception v3 as the CNN architecture. We developed an automatic microscopy image acquisition system, enabling us to obtain 154 images for 7 min. Over 12,000 images of aggregated and dispersed flocs were obtained from wastewater treatment plant (WWTP)-S and -E over 15 weeks. Clasifier-1 was retrained using these images. Clasifier-1 distinguished the aggregated and dispersed flocs with a training accuracy of approximately 95% and recognized a 20% morphological change in the aggregated flocs. Classifier-1 also recognized the morphology of AS flocs obtained from other WWTPs, the AS from which was used for retraining. Classifier-2 quantitatively recognized an abundance of filamentous bacteria in the AS flocs. These results clearly indicated that the developed image classification model could serve as a useful warning system for the settleability deterioration and abundance of filamentous bacteria in the aeration tank of a full-scale AS system.

1. Introduction

Activated sludge (AS) systems are the most common type of biological wastewater treatment technology and are applied worldwide. AS contributes to the biological conversion of contaminants in AS systems. AS consists of a complex microbial ecosystem composed of a variety of microorganisms (filamentous and floc-forming bacteria, protozoa, and metazoa) and abiotic elements (extracellular polymers and debris) 1,2. These components form a floc, the physical structure of which reflects the water quality and operating conditions of the wastewater treatment system. Owing to the complex nature of microbial communities in a floc, imbalances may occur among the different microorganisms, thereby leading to a change in the floc structure. This causes a serious deterioration in the performance of AS systems, with profound economical and environmental consequences owing to the strict regulations regarding effluent quality. Therefore, the detection of disturbances is definitely an important task for the stability and enhancement of process performance in wastewater treatment plants (WWTPs) 3.

A major drawback of AS systems that is relevant to the floc structure is the poor settling ability of the AS for separation from the treated effluent by settling in the secondary sedimentation tank. This is associated with the loose structure and lower density (that is, bulking), which frequently results in sludge washout with the final effluent, consequently causing poor effluent quality as well as deteriorated dewatering and thickening sludge properties 4–6. Therefore, the sludge settling ability is crucial to the efficient operation of the AS system, and it is commonly quantified by the sludge volume index (SVI). Various factors, such as the AS flocculation, stability, aggregate size, morphology, density, and chemical composition, affect the AS floc settling ability 5. Some of these factors can be visualized by microscopy inspection, which is a

very useful method for the rapid diagnosis of AS process malfunctions 7. The regular monitoring of the microscopic parameters of AS flocs may provide important information regarding the dynamic changes in the water quality and operational parameters of an AS system. Correlations have been identified between the AS floc properties and operational conditions. These include the biochemical to chemical oxygen demand ratio (BOD:COD), carbon to nitrogen ratio (C:N), toxic compounds inhibition, hydraulic and sludge loading rate, recirculation ratio, aeration equipment, substrate uptake rate, oxygen uptake rate, treatment efficiency, excess sludge production, and SVI 1. Therefore, it is generally considered that the characterization of AS flocs by microscopy inspection can provide important information regarding the biological processes leading to the operational conditions of an AS system. However, automatic AS floc classification is desirable, as the acquisition of information relating to the morphology of AS flocs from microscopy inspection results requires skilled and specialized expertise.

In this sense, microscopy techniques coupled with quantitative image analysis (QIA) of AS flocs may offer an advantage for the prediction purposes of an AS system. QIA applications have been employed for the determination of the aggregated and filamentous bacteria contents as well as the floc structure to assess the AS operating parameters 1,3,8–11. All of the studies mentioned above demonstrated that image processing and analysis methodologies could provide valuable morphological information (for example, the surface, area, perimeter, perimeter/area ratio, circularity, minimum and maximum caliper diameter, and specific filament length 1) as well as physiological information (such as the Gram-positive/Gram-negative and viable/damaged bacteria ratios 3) on AS flocs, particularly in terms of the characteristics of filamentous bacteria 8,9. Therefore, at present, such technologies are recognized as valid monitoring tools 3. Indeed,

the possibility of accurately monitoring the filamentous bacteria contents, and of characterizing and quantifying the aggregated biomass contents, size stratification, and structure using such simple, quantitative, automated, and near-real-time methodology, overwhelms the conventional monitoring methods.

Although the current QIA technologies described above are quite powerful tools for analyzing the physical properties of AS flocs, these require extensive pre-processing of images, such as object segmentation, background determination and removal, debris elimination, and image enhancing operations 3,5,8. This process is laborious and time consuming, and may pose the risk of subjective definitions (differences of appreciation between operators) of the threshold values for the differentiation between the objects and background 5, which may also lead to important information being discarded. Furthermore, the International Water Association Digital Water Group emphasizes the importance of the development of new systems based on cyber-physical systems, digitalization, and big data to enable informed decisions in increasingly changing, complex, and uncertain water issues 12. In this context, the currently available QIA technologies are semi-automated techniques used by human researchers, and alternative technology is urgently required to extract the discriminant features from the images automatically by removing subjectivity.

The logical next step is to allow computers to learn the features that optimally represent the images. This concept forms the basis of many deep learning algorithms in which models (networks) are composed of numerous layers that transform the input data (such as images) into outputs (for example, the probability of being classified into an appropriate label) 13. Deep

learning is a learning approach that automatically learns the feature representations from raw data without any pre-processing. The most successful type of model for image analysis to date is the convolutional neural network (CNN) 14. CNNs contain many layers that transform their input with convolutional filters of a small extent. Extensive work has been conducted on CNNs, which have been applied, for example, to medical image analyses 13. Researchers have applied CNNs to large-scale image classification tasks to address problems in civil and environmental engineering 15–17. Dung and Anh developed a vision-based method for concrete crack detection and density evaluation 18. Their method identified the crack path with an average precision of approximately 90%. Wu et al. constructed a CNN to classify images of the surfaces of fountains, lakes, oceans, and rivers into sub-categories of clean and polluted water 19. They concluded that the proposed CNN could substantially decrease the manual burden of users in observing the images of surveillance cameras. Yurtsever and Yurtsever achieved the automatic classification of microplastics in water and wastewater based on numerous microscopic images using a CNN 20. The classification revealed accuracy rates of 97% and 89% for microbeads in pure water and wastewater, respectively.

Inspired by the success of CNNs for image classification tasks, in this study, we used a CNN-based method to achieve the automatic classification of AS flocs in full-scale WWTPs based on morphological properties. We selected Inception v3 as the CNN architecture, which is a network that is pre-trained on a large-scale image classification task 21. Firstly, we developed an automatic microscopy image acquisition system using only free software to obtain a sufficient number of training images. Using the images, two types of two-label classifiers were developed for recognizing aggregated or dispersed flocs and the presence or absence of filamentous

bacteria. The sensitivity of the classifier was estimated and the weekly changes in the morphological characteristics of the AS flocs in WWTPs were investigated. Furthermore, the versatility of the classifier was confirmed by analyzing the morphology of AS flocs obtained from six different WWTPs. The evolution of filamentous bacteria in the AS was also analyzed using another classifier and was correlated to the SVI values. In all of the tests, the results of the classification conducted by the classifiers were compared with those obtained by humans.

2. Materials and Methods

AS samples

In this study, the AS samples were collected from aeration tanks in eight WWTPs, denoted by S, E, N, M, Sh, H, K, and T, in five prefectures of Japan, all of which predominantly treat domestic wastewater, between September 30th, 2019 and January 28th, 2020. A total of 40 mL of the sample was collected in a 50 mL sterile Falcon tube, transferred to our laboratory at 4 °C with neither feeding nor aeration, and subjected to image analysis within 2 days of the sample collection. The physicochemical parameters of the AS samples and liquid in the aeration tanks during a test period are described in Table S1. WWTP-S, -Sh, and -T were identical to WWTP-A, -B, and -C described in a previous study 22.

Automatic acquisition of AS floc images

For the AS microscopic inspection, four 50 μL aliquots of mixed liquor were randomly sampled from each AS sample. The sample was carefully placed on a glass slide by means of a calibrated micropipette with a sectioned tip to minimize the disruption of the native floc characteristics and to allow the largest AS floc to pass through. Thereafter, the sample was

covered with a coverslip (18 × 18 mm). The slide was fixed on a high-precision motorized XY stage (mmu-60x; Chuo Precision Industrial Co., Ltd., Tokyo, Japan) 23. The XY stage with the slide and the tabletop digital microscope (UM06; Kenis Ltd., Osaka, Japan) were covered with a small darkroom. The slide was illuminated by a white LED light from a smartphone from the back. We took images of floc under the same light condition to eliminate difference of color of flocs among samples. The structure of the low-cost microscope and stage is presented in S1. All digital images of the AS flocs on the slide were acquired with the digital microscope. The tabletop digital microscope, which is commercially designed for classrooms, is manually driven and lacks the ability to capture images automatically. Therefore, we installed free software (UM6-CAM and Keytokey) on a computer to store images automatically every 3 s at a resolution of 640 × 480 pixels with a corresponding area of 1.44 × 1.09 mm in a 24-bit JPEG image. Furthermore, to capture numerous digital images of the AS flocs on the slides automatically, we combined the microscope with the high-precision motorized XY stage described above, which was controlled by a control driver (CAT-D 3-axis controller; Chuo Precision Industrial Co., Ltd., Tokyo, Japan) connected to a computer with free software (cat-cd3 and Keytokey) installed. The field of view automatically meandered from the upper left corner to the lower right corner of the object, which was adjusted stepwise to the next non-overlapped field of view every 3 s (Figure S1). A total of 154 (14 × 11) images per slide were exhaustively acquired, which covered 73% of the entire area of the object. Six slides were prepared so that a total of 924 images were acquired per sample.

Devices, software, and models

In this study, we used an OptiPlex 7040 computer with the Windows 10 operating system (version 1909). This machine has a 3.4 GHz Intel Core i7-6700 CPU processor and 8 GB 1,600 MHz DDR3 of RAM memory. Oracle VM VirtualBox version 6.0.14, which is a free and open-source hosted hypervisor, was downloaded and installed. Thereafter, Ubuntu 16.04, which is an open-source software operating system, was installed in VirtualBox. Furthermore, TensorFlow 1.11.0 with Python 2.7.12 bindings was installed and executed, with the following tools downloaded and installed 24: (i) TensorFlow Hub was installed through the terminal with the following instruction: "pip install tensorflow-hub" 24. TensorFlow Hub is a library for reusable machine learning modules. (ii) The code retrain.py was downloaded 25. This code allows the pre-trained Inception network to be adapted to other classification problems. (iii) The code label_image.py was downloaded 26. This code uses the Inception v3 model to classify images that are passed to the model (a classifier) from the command line. These instructions indicate the script that carries out the retraining (retrain.py) and classification (label_image.py) on the Inception model. The Inception v3 model consists of a 22-layer network with 24M parameters. Moreover, it indicates the labels that are used for training: WWTP-S and WWTP-E for Classifier-1 or the absence and presence of filamentous bacteria for Classifier-2. The command line used to retrain the Inception v3 model and to classify the images into the two classes is illustrated in Figure S2. The path where the pictures could be found was as follows: --image=sample/Sample001.jpg. In this path, there were two directories: one with the images of WWTP-S for Classifier-1 (the absence of filamentous bacteria for Classifier-2) and another with the images of WWTP-E for Classifier-1 (the presence of filamentous bacteria for Classifier-2). The AS floc image for evaluation was selected and classified into one of two classes described above, and displayed quantitatively with a certain probability.

3. Results and Discussion

Characteristics of AS flocs

Figure 1 presents typical images of the AS flocs obtained from WWTP-S and WWTP-E (see also Figure S3). The AS flocs exhibited marked morphological differences between the two WWTPs. The shape, structure, and strength of the AS flocs were considered to be three important morphological characteristics 5,7. According to this definition, the AS flocs from WWTP-S exhibited an irregular shape, a compact structure, and a dark color. These were firm flocs and the surrounding liquid was clear. In contrast, the AS flocs from WWTP-E exhibited an open structure and a light color (Figure 1). These were weak flocs, which were less dense and particularly highly dispersed. As these weak flocs were connected to one another, individual flocs could not be identified (Figure S3). The surrounding liquid was turbid, with pinpoint flocs and small particles. The results could be explained by the difference in the physicochemical parameters between the WWTPs. The physicochemical parameters of the WWTPs during the test period are presented in Figure 2 and listed in Table S1. All three parameters relevant to the sludge properties (mixed liquor suspended solids (MLSS), the sludge volume occupied by settled sludge after 30 minutes (SV30), and SVI) were higher in WWTP-E than in WWTP-S, indicating that AS bulking occurred in WWTP-E. Many studies have suggested that the threshold value for activated sludge bulking was an SVI value of around 150 mL/g 27. The SVI values of WWTP-S were only below the threshold. In contrast, the average SVI value was highest in WWTP-E so that we selected WWTP-S and WWTP-E samples for the representation of aggregated and dispersed flocs.

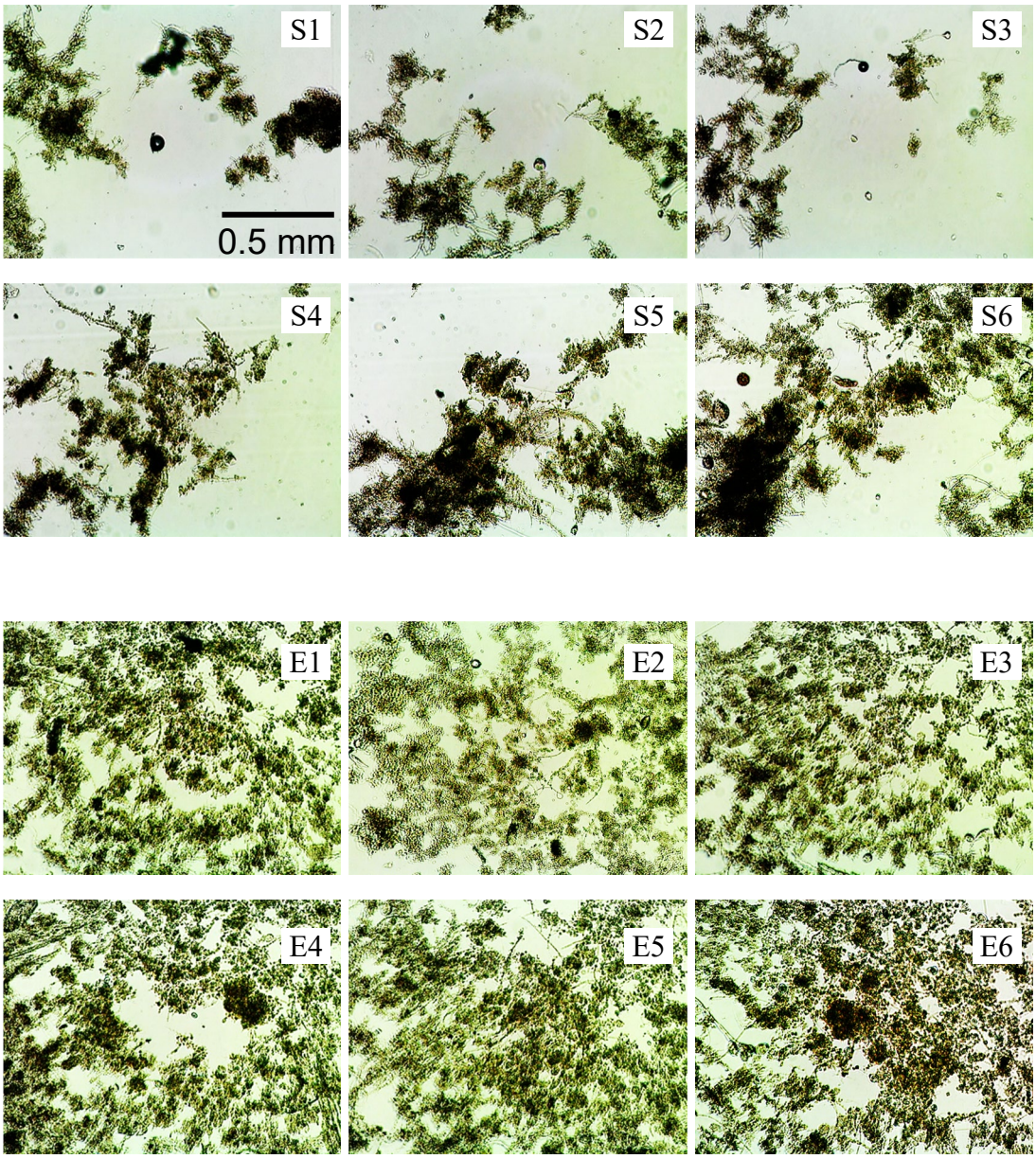

Figure 1. Typical microscopic images in bright field of AS flocs obtained from WWTP-S (S1 to S6) and WWTP-E (E1 to E6).

225

226

227

228

229

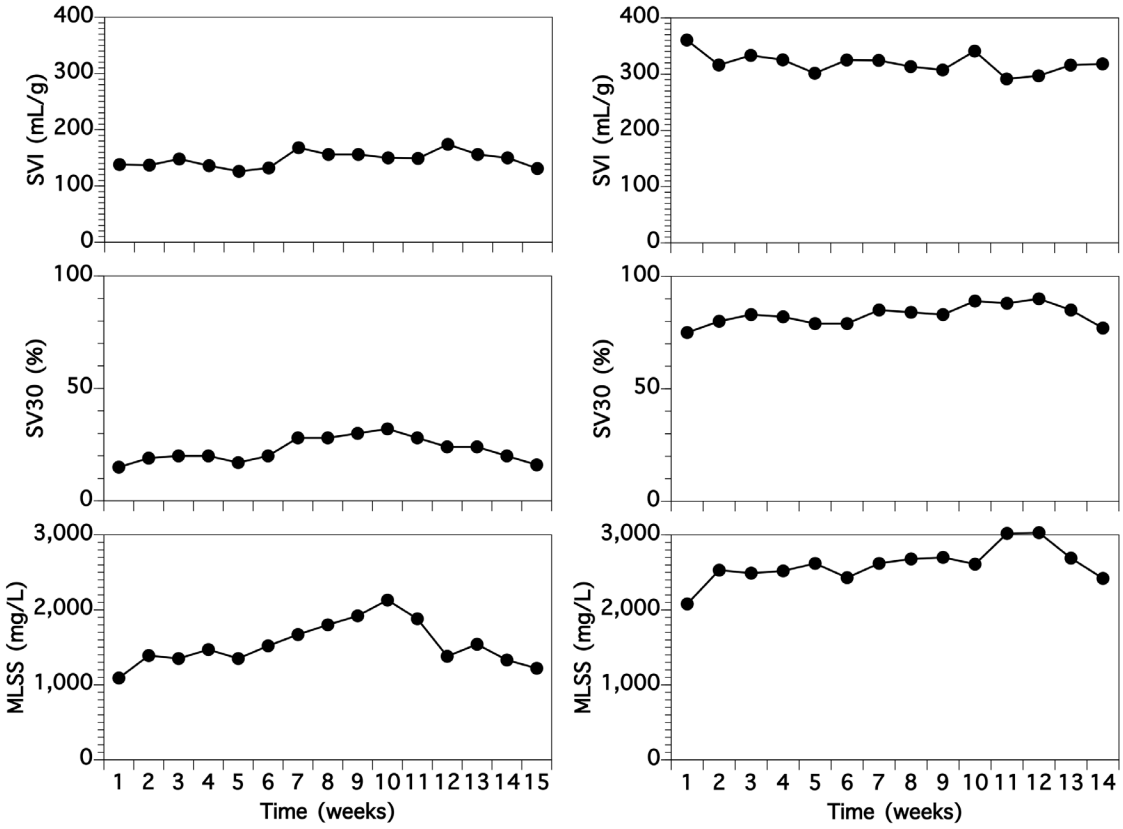

Figure 2. SVI, SV30, and MLSS of WWTP-S (left panels) and WWTP-E (right panels) during test period.

230

231 Development of image classification model and evaluation of training performance

232 To develop the image classification model (Classifier-1), we obtained AS samples over 15

233 weeks, and eventually accumulated 13,860 images of AS flocs for WWTP-S and WWTP-E. A

234 split of 83%/17% was used for the training and test sets. The first step was to evaluate the

235 training performance. In this study, we used the TensorFlow framework. TensorBoard is a

236 TensorFlow histogram and graph visualization tool to ensure that the intended design is achieved

237 28. Figure S4 indicates training accuracy of approximately 95% achieved in distinguishing the

238 images of the AS flocs obtained from WWTP-S from those obtained from WWTP-E.

239

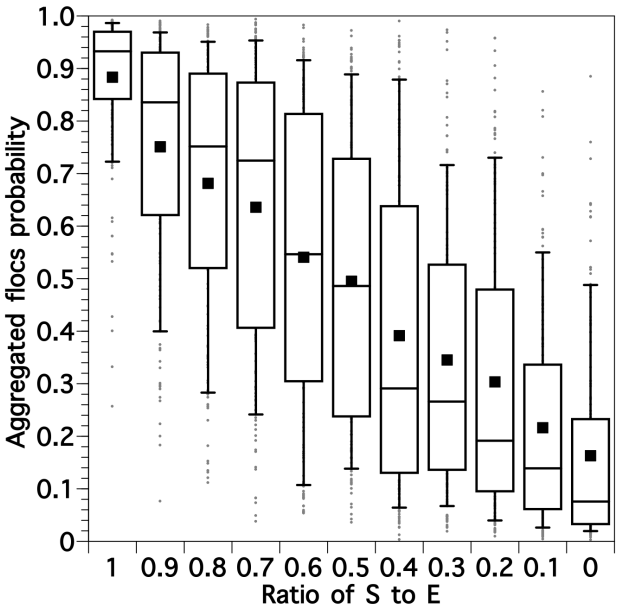

Figure 3. Boxplot of average aggregated flocs probability score of 154 images of AS flocs at various mixing ratios between AS from WWTP-S and WWTP-E. The rectangular box indicates the lower and upper quartiles and the median, the square plot indicates the average, and the whiskers indicate the 9th percentile and the 91st percentile. All other results are plotted as outliers.

240

241 Sensitivity analysis of Classifier-1

242 Prior to classifying the images of the AS flocs obtained from WWTP-S and WWTP-E, we
243 investigated the sensitivity with which Classifier-1 could recognize the morphology (for
244 example, the shape, structure, strength, and color) of the AS flocs. AS samples with different
245 morphologies were prepared by mixing AS sludge samples obtained from two WWTPs at
246 different volume ratios. The average aggregated flocs probability score of 154 images of the AS
247 flocs from WWTP-S (that is, a ratio of 10:0) was 0.88 (Figure 3). As the volume ratio of the AS
248 sample from WWTP-E to that from WWTP-S increased, the average probability score decreased
249 linearly. Statistical analysis was conducted using the two-tailed student's t-test. The pair-to-pair
250 p-values between 10% change of the volume ratio of the AS sample ranged from 0.057 to 0.51,

indicating that Classifier-1 could not recognize the change in morphology of the AS flocs. In contrast, the pair-to-pair p-values between 20% change of the volume ratio of the AS sample were <0.007, indicating that Classifier-1 could recognize the 20% change in morphology of the AS flocs. The slope of the linear regression line of the average probability scores was estimated using Microsoft Excel. The change rate of the average probability score per 100% change in the sample volume was 0.69 with the correlation coefficient of the linear regression of average probabilities of 0.996. These results indicated that the change in 0.138 of the average probability score suggested the occurrence of a 20% morphological change in the original AS flocs of WWTP-S.

We could also evaluate the recall based on the data at 1.0 of the S/E ration shown in Figure 3. Defining that the result with >0.8 of the probability was positive, the recall was calculated to be 0.83.

To date, deep learning technologies have been applied successfully in various fields of civil and environmental engineering with significant progress in machine learning techniques 15,17. However, a critical factor that hampers the popularization of this technology in civil and environmental engineering, particularly wastewater treatment systems, may be the necessity to develop a program (or modify a existing program) that is adequate for the user's purpose 19,29. Engineers of WWTPs are usually unfamiliar with writing a program. However, as demonstrated above, the unmodified Inception v3 model could achieve classification of the morphology of AS flocs with high sensitivity. This is because the two labels we adopted in this study were AS flocs with a compact or dispersed structure and in the presence/absence of filamentous bacteria (see

below), which could easily be distinguished even by human eyes. Therefore, we are convinced that the development of a novel deep learning program is not necessarily required to address simple issues in AS systems. Another means of successfully achieving the classification of the morphology of AS flocs could be to adopt Inception v3 as CNN architecture. Inception v3 is open-source architecture developed by Google, and it is a CNN that is 48 layers deep. A pre-trained version of the network trained on more than one million images from the ImageNet database can be loaded. The pre-trained network can classify images into 1000 object categories, such as keyboard, mouse, pencil, and many animals. As a result, the network has learned rich feature representations for a wide range of images and is particularly suitable for large-scale image classification tasks 21. However, these characteristics adversely become a drawback because we cannot easily develop the purpose-designed model.

Classification of morphology of AS flocs with classifier-1

Subsequently, we attempted to recognize the weekly change in the morphological characteristics of the AS flocs using the classifier. Figure 4 presents the average aggregated flocs probability score of the tested AS flocs obtained from WWTP-S for 15 weeks (not sampled at the 9th week). The average probability score for 15 weeks was 0.936. All of the averaged probability scores were >0.798 (0.936–0.138). This indicated that the morphological characteristics of the AS flocs did not change in a degree of >20% to dispersed and light-colored ones compared to the usual ones. Figure 2 shows that both the SVI and SV30 of WWTP-S were stable for 15 weeks, which supported the results of investigation with classifier-1.

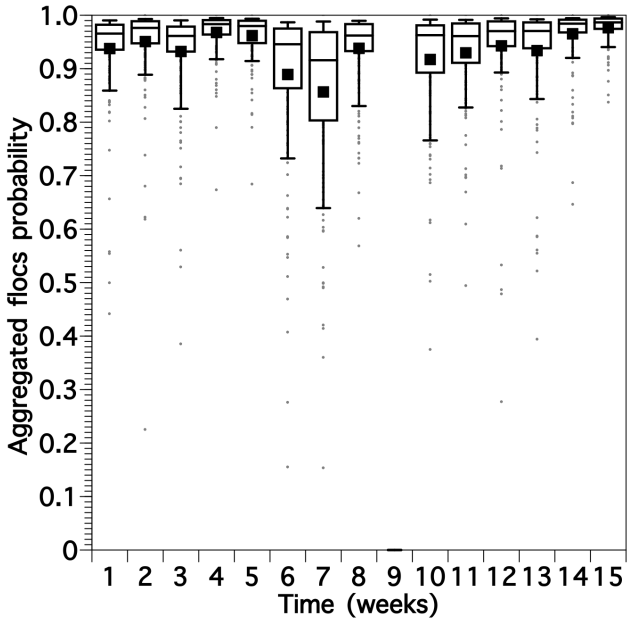

Figure 4. Boxplot of average aggregated flocs probability scores of 154 images of AS flocs obtained from WWTP-S over 15 weeks. The rectangular box indicates the lower and upper quartiles and the median, the square plot indicates the average, and the whiskers indicate the 9th and 91st percentiles. All other results are plotted as outliers.

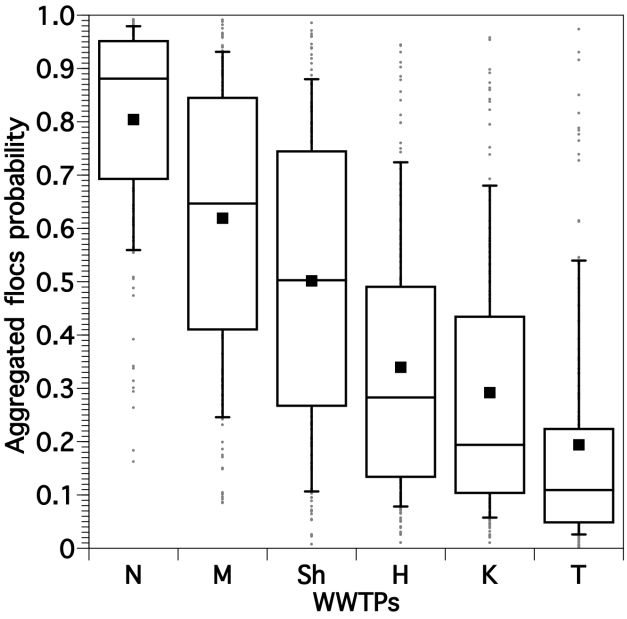

Figure 5. Boxplot of average aggregated flocs probability scores of 154 images of AS flocs obtained from six different WWTPs. The rectangular box indicates the lower and upper quartiles and the median, the square plot indicates the average, and the whiskers indicate the 9th and 91st percentiles. All other results are plotted as outliers.

297

298

Furthermore, we attempted to recognize the distinct morphological changes in the flocs from WWTP-S. As we could not obtain flocs with clearly different morphological characteristics (for example, open, light-colored, less dense or dispersed flocs) from the full-scale WWTP-S, the AS was cultivated in our laboratory with vigorous aeration to disperse the floc structure intentionally. The SVI of the flocs prior to the cultivation was 78 mL/g. The SVI increased to 128 mL/g after 1 day and to 157 mL/g after 2 days of cultivation, indicating poor settleability. The microscopy inspection demonstrated that the flocs were dispersed and their size decreased (Figure S5). The averaged probability scores decreased significantly from 0.94 to 0.38 during 2 days of cultivation (Figure S6), indicating that Classifier-1 could recognize the morphological changes (mainly dispersion) in the flocs from WWTP-S even though the images originated from WWTP-E were used for the retraining of Classifier-1.

To investigate the versatility of the classifier developed in this study, we applied Classifier-1 to recognizing the morphology of AS flocs obtained from WWTPs other than WWTP-S and -E. The order of the averaged aggregated flocs probability scores from highest (similar to WWTP-S) to lowest (similar to WWTP-E) was WWTP-N, M, Sh, H, K, and T (Figure 5). Images of the flocs obtained from these WWTPs were shown in Table S1. The flocs from WWTP-N exhibited a compact structure and dark color. These were firm flocs and the surrounding liquid was clear, and these characteristics were quite similar to those of the flocs from WWTP-S. In contrast, the flocs from WWTP-T exhibited an open structure and a light color. These were weak flocs, which were less dense and highly dispersed, and the surrounding liquid was turbid. Their characteristics were quite similar to those of the flocs from WWTP-E. The flocs from WWTP-H and WWTP-K exhibited similar morphologies to those of the flocs from WWTP-E and WWTP-T but the

density of the flocs from WWTP-H and WWTP-K appeared to be lower than that of the flocs from WWTP-E and WWTP-T. In particular, the flocs from WWTP-K were connected to one another with filamentous bacteria so that individual flocs could not be identified. The flocs from WWTP-M and WWTP-Sh exhibited similar morphologies to those of the flocs from WWTP-S and WWTP-N, but the color of the flocs from WWTP-M and WWTP-Sh appeared to be lighter than that of the flocs from WWTP-S and WWTP-N. A comparison of the results obtained from the analysis by Classifier-1 and the microscopy inspection revealed that the estimation of the averaged probability scores by Classifier-1 evidently enabled the classification of the morphological similarity of the flocs from each WWTP into two morphologically distinct labels.

However, the order of the density of the AS flocs described above (Figure 5) was not completely identical to the order of SVI: S < Sh = T < M < E (Table S1). This was also probably because parameters other than the morphology of the flocs could influence the SVI. An improvement in the correlation between the results from a classifier and conventional water quality monitoring could be achieved by selecting a training dataset that is more appropriate for the purpose.

Classification of filamentous bulking occurrence with classifier-2

Furthermore, we attempted to develop an early warning system for the occurrence of filamentous bulking in an AS system. To achieve this, we constructed a new classifier (Classifier-2). AS samples were obtained from December 10th, 2019 to January 28th, 2020 at WWTP-M, where filamentous bulking has occurred every winter. In this case, 924 images were acquired per sample, as described above. We gathered AS samples at 6 weeks. A split of 75%/25% of images at the 1st (December 10th) and 4th (January 14th) weeks was used for the training and test sets,

345 respectively, because the abundance of filamentous bacteria was the lowest at the 1st week and
346 additional filamentous bacteria were found at the 4th week (see Figure S8) and the SVI of the AS
347 were 191 mL/g and 352 mL/g, respectively. Therefore, the images at the 1st and 4th weeks were
348 used to retrain Classifier-2 and were used as the two respective classification labels (the absence
349 or presence of filamentous bacteria).
350
351 The SVI of the AS of WWTP-M fluctuated from 120 mL/g to 270 mL/g by the middle of
352 December, whereas it increased gradually thereafter (Figure S7). It reached the peak at the
353 middle of January and then decreased slightly. Figure S8 presents images of the flocs obtained
354 from WWTP-M during the test period. The abundance of filamentous bacteria increased
355 obviously over time from December 10th to January 14th, and it was comparable thereafter. The
356 averaged bulking probability score was 0.85 on December 10th, with a sudden decrease to 0.47
357 on December 24, and it was comparable thereafter (Figure 6). The correlation coefficient
358 between the averaged bulking probability score and the SVI over the operational period was
359 0.67. Thus, Classifier-2 developed in this study could detect the abundance of filamentous
360 bacteria in AS flocs, which was roughly correlated with the SVI.
361
362

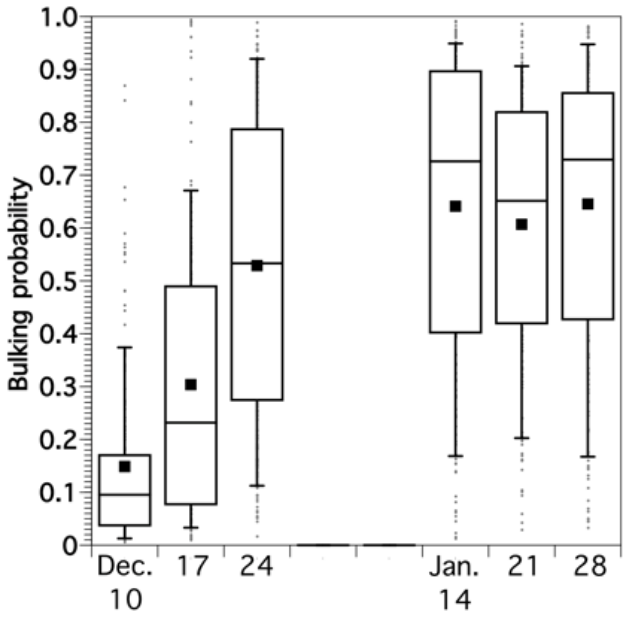

Figure 6. Boxplot of average bulking probability scores of 154 images of AS flocs obtained from WWTP-M. The rectangular box indicates the lower and upper quartiles and the median, the square plot indicates the average, and the whiskers indicate the 9th and 91st percentiles. All other results are plotted as outliers.

4. Conclusions

We developed an image classification model (classifiers) using a CNN-based method. Clasifier-1 distinguished the aggregated flocs from the dispersed ones with high training accuracy (approximately 95%) and could recognize 20% morphological changes in the aggregated flocs to dispersed ones. We selected the pre-trained Inception v3 as the CNN architecture. Inception v3 is open-source architecture developed by Google and is a widely used image recognition model. As it has been trained on more than one million images from the ImageNet database, we could use it without any modification or adaptation for the recognition of AS flocs. These findings imply that the features of Inception v3 can accelerate the popularization of deep learning-based image classification technology to analyze digital images obtained in an AS system automatically. We could develop an automatic microscopy image acquisition system

with an inexpensive microscope, and are currently developing an auto-sampler of mixed liquor in an aeration tank and a microfluidic device for automatic image acquisition. In the future study, we will develop a single simple coherent system. Eventually we will develop a useful warning system for the settleability deterioration and abundance of filamentous bacteria in the aeration tank of an AS system in the near future, which will contribute to the stability and even improvement in the performance of wastewater treatment processes.

Acknowledgements

We are grateful to Mr. Tsuyoshi Kurita and Mr. Shinsuke Hamada for their valuable comments on microscopy inspection. This research did not receive any specific grant from funding agencies in the public, commercial, or not-for-profit sectors.

REFERENCES

1 A. Gnida, Archives of Environmental Protection, 2017, 43 (4), 66–71.

2 J. S. Guo, F. Fang, P. Yan and Y. P. Chen, Bioresource Technology, 2020, 297, 122506.

3 D. P. Mesquita, A. L. Amaral and E. C. Ferreira, Chemical Engineering Journal, 2016, 285, 349–357.

4 E. G. W. Gunawardana, H. Satoh and T. Mino, Journal of Water and Environment Technology, 2014, 12, 1–12.

5 D. P. Mesquita, A. L. Amaral and E. C. Ferreira, Analytica Chimica Acta, 2013, 802, 14–28.

6 C. Ye, X. Yang, F. J. Zhao and L. Ren, Bioresource Technology, 2016, 207, 11–18.

7 D. H. Eikelboom, Process control of activated sludge plants by microscopic investigation, IWA Publishing, London, 2000.

8 W. Burger, K. Krysiak-Baltyn, P. J. Scales, G. J. O. Martin, A. D. Stickland and S. L. Gras, Water Research, 2017, 123, 578–585.

9 K. Campbell, J. Wang and M. Daniels, Chemosphere, 2019, 223, 694–703.

10 E. Koivuranta, T. Stoor, J. Hattuniemi and J. Niinimäki, Journal of Water Process Engineering, 2015, 5, 28–34.

11 P. Oliveira, M. Alliet, C. Coufort-Saudejaud and C. Frances, Water Science and Technology, 2018, 77, 2415–2425.

12 The IWA Digital Water Group, Towards the Next Generation of Water Systems, https://iwa-network.org/projects/digital-water-programme/#why_digital_water?_, (accessed 6 October 2020).

13 G. Litjens, T. Kooi, B. E. Bejnordi, A. A. A. Setio, F. Ciompi, M. Ghafoorian, J. A. W. M. van der Laak, B. van Ginneken and C. I. Sánchez, Medical Image Analysis, 2017, 42, 60–88.

14 Y. LeCun, Y. Bengio and G. Hinton, Nature, 2015, 521, 436–444.

15 Y. Huang, J. Li and J. Fu, CMES-Computer Modeling in Engineering and Sciences, 2019, 121, 845–875.

16 H. Yamamura, E. U. Putri, T. Kawakami, A. Suzuki, H. D. Ariesyady and T. Ishii, Separation and Purification Technology, 2020, 237, 116467.

17 X. W. Ye, T. Jin and C. B. Yun, Smart Structures and Systems, 2019, 24, 567–585.

18 C. V. Dung and L. D. Anh, Automation in Construction, 2019, 99, 52–58.

19 Y. Wu, X. Zhang, Y. Xiao and J. Feng, Applied Sciences (Switzerland), 2020, 10, 909.

20 M. Yurtsever and U. Yurtsever, Chemosphere, 2019, 216, 271–280.

21 C. Szegedy, V. Vanhoucke, S. Ioffe, J. Shlens and Z. Wojna, in Proceedings of the IEEE Computer Society Conference on Computer Vision and Pattern Recognition, 2016, pp. 2818–2826.

22 H. Satoh, K. Kikuchi, Y. Katayose, S. Tsuda, R. Hirano, Y. Hirakata, M. Kitajima, S. Ishii, M. Oshiki, M. Hatamoto, M. Takahashi and S. Okabe, Science of the Total Environment, 2020, 715, 136928.

23 S. Okabe, H. Satoh and Y. Watanabe, Applied and Environmental Microbiology, 1999, 65 (7), 3182–3191.

24 M. A. Espinoza, G. H. Alférez and J. Castillo, in International Conference on Health Informatics and Medical Systems, Las Vegas, Nevada, USA, 2018, pp. 90–95.

25 GitHub, tensorflow / hub, https://github.com/tensorflow/hub, (accessed 6 October 2020).

26 GitHub, tensorflow / tensorflow, https://github.com/tensorflow/tensorflow, (accessed 6 October 2020).

27 A. J. Schuler and D. Jassby, Water Research, 2007, 41, 4349–4356.

28 GitHub, tensorflow / tensorboard, https://github.com/tensorflow/tensorboard, (accessed 6 October 2020).

29 X. Zhou, Z. Tang, W. Xu, F. Meng, X. Chu, K. Xin and G. Fu, Water Research, 2019, 166, 115058.

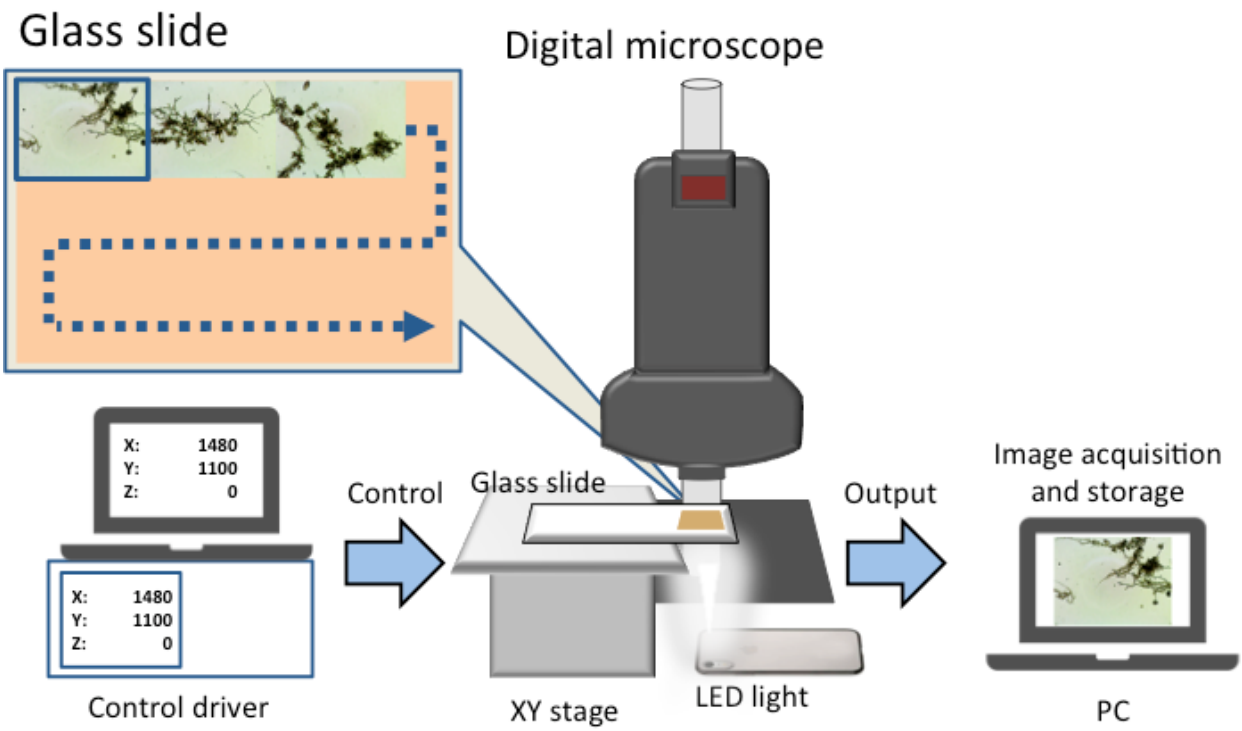

Figure S1. Schematic representation of automatic microscopy image acquisition system.

```
# call retrain.py

source ~/tensorflow/venv/bin/activate

cd ~/tensorflow/retrain

python retrain.py \
  --bottleneck_dir=tmp/bottlenecks \
  --how_many_training_steps=100 \
  --model_dir=tmp/inception \
  --summaries_dir=tmp/training_summaries/basic \
  --output_graph=output/retrained_graph.pb \
  --output_labels=output/retrained_labels.txt \
  --image_dir=test_data

# classify images

source ~/tensorflow/venv/bin/activate

cd ~/tensorflow/retrain

python label_image.py \
  --graph=output/retrained_graph.pb \
  --labels=output/retrained_labels.txt \
  --input_layer=Placeholder \
  --output_layer=final_result \
  --image=sample/Sample001.jpg
```

Figure S2. Command line used to retrain Inception v3 model and to classify images into one of two classes.

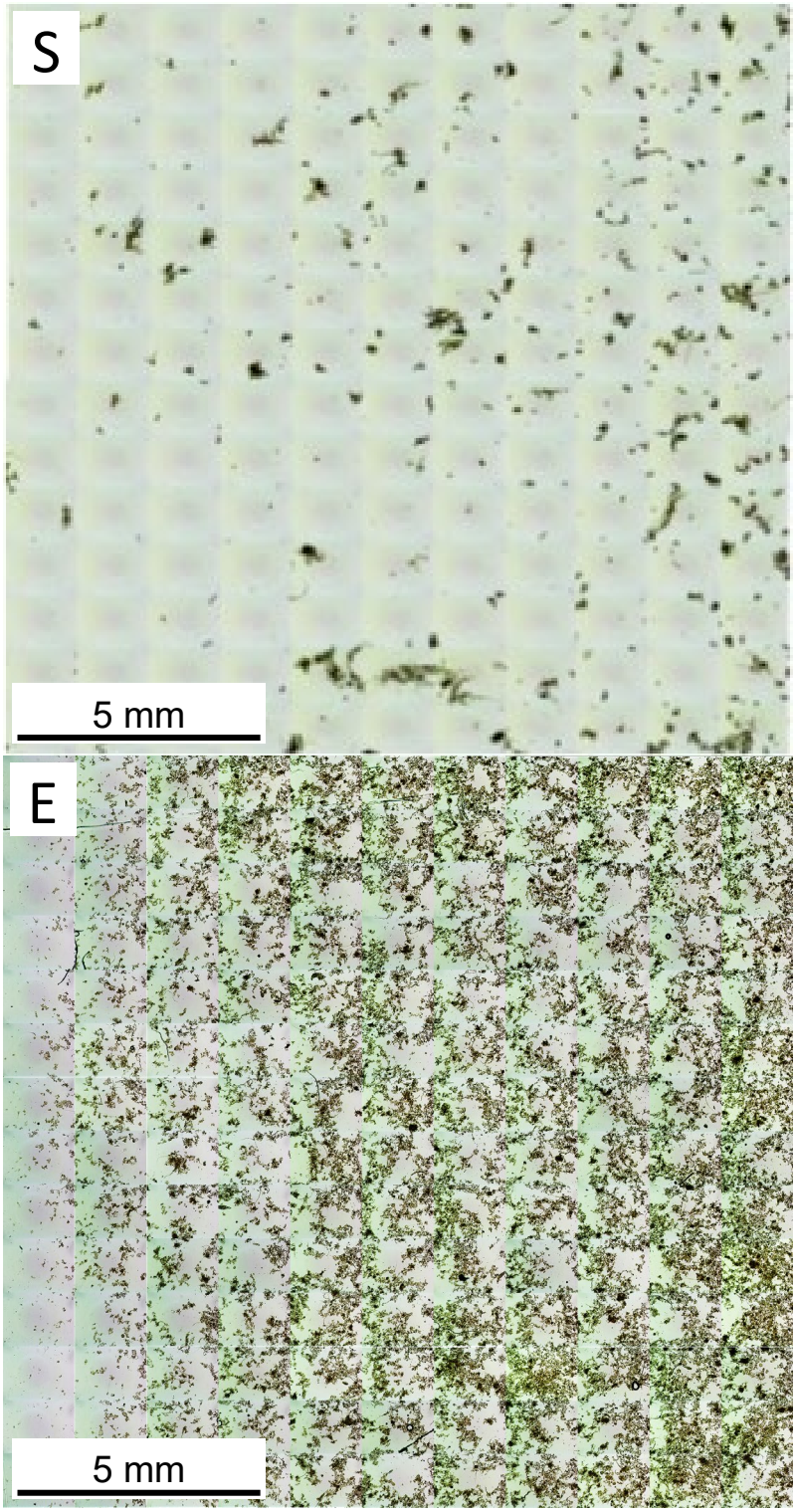

Figure S3. Typical microscopic images in bright field of AS flocs obtained from WWTP-S (S) and WWTP-E (E). A total of 154 were exhaustively acquired in a single slide and assembled. Small gaps between images were closed.

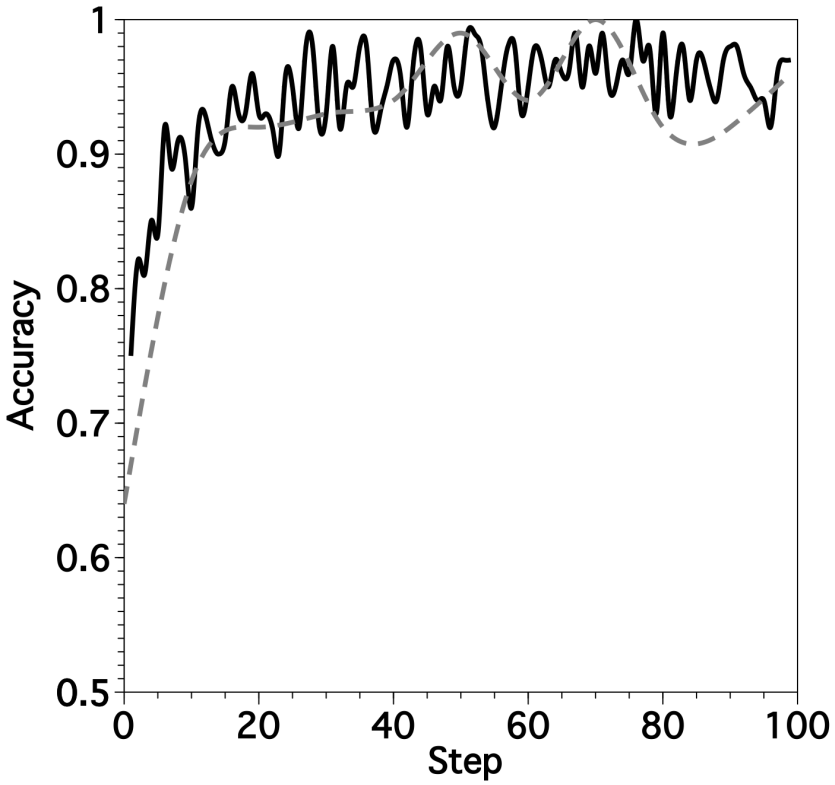

Figure S4. Training (solid line) and validation (dashed line) accuracy for Classifier-1 during 100 training steps.

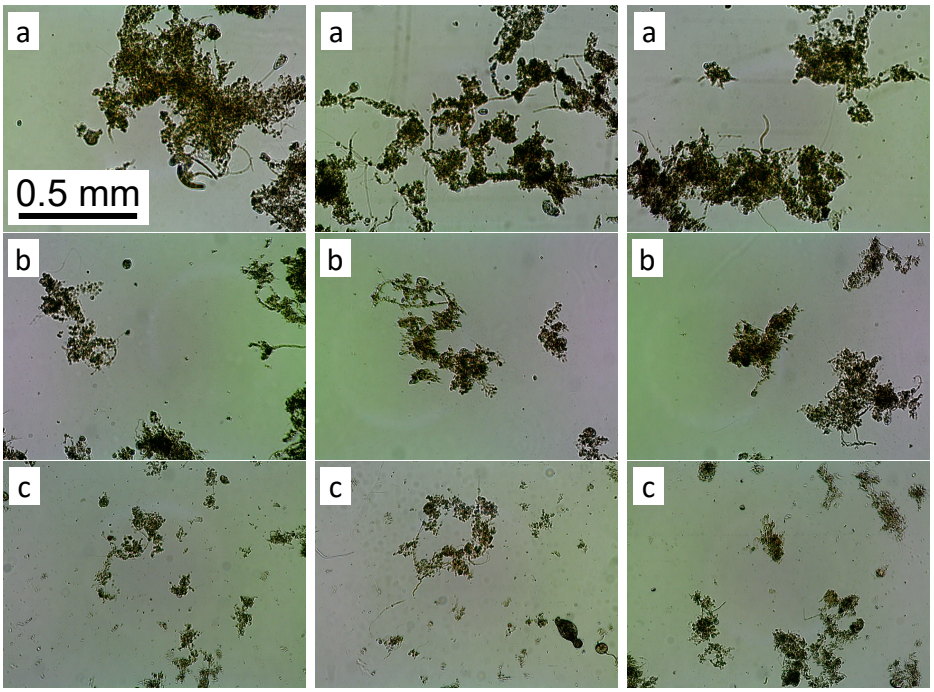

Figure S5 Typical microscopic images in bright field of AS flocs obtained from WWTP-S at (a) day 0, (b) day 1, and (c) day 2.

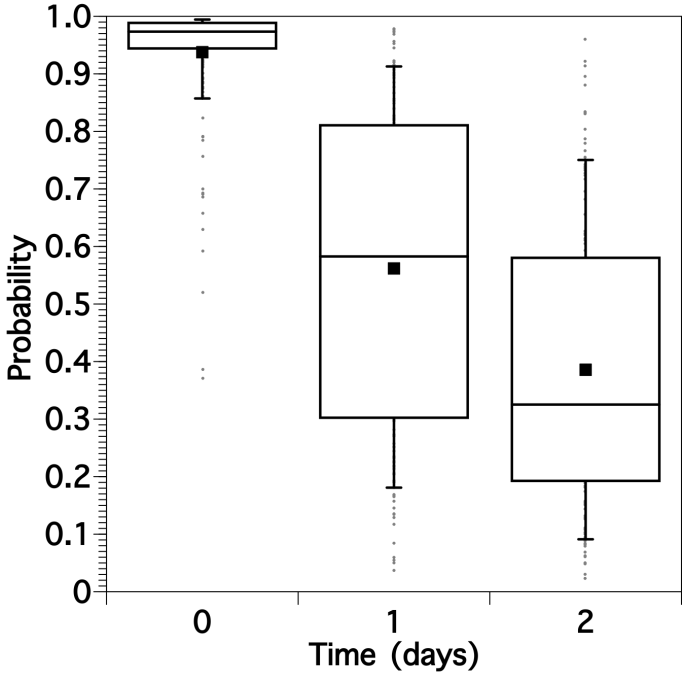

Figure S6. Boxplot of average probability scores of 154 images of AS flocs obtained from WWTP-S and cultivated in our laboratory with vigorous aeration. The rectangular box indicates the lower and upper quartiles and the median, the square plot indicates the average, and the whiskers indicate the 9th and 91st percentiles. All other results are plotted as outliers.

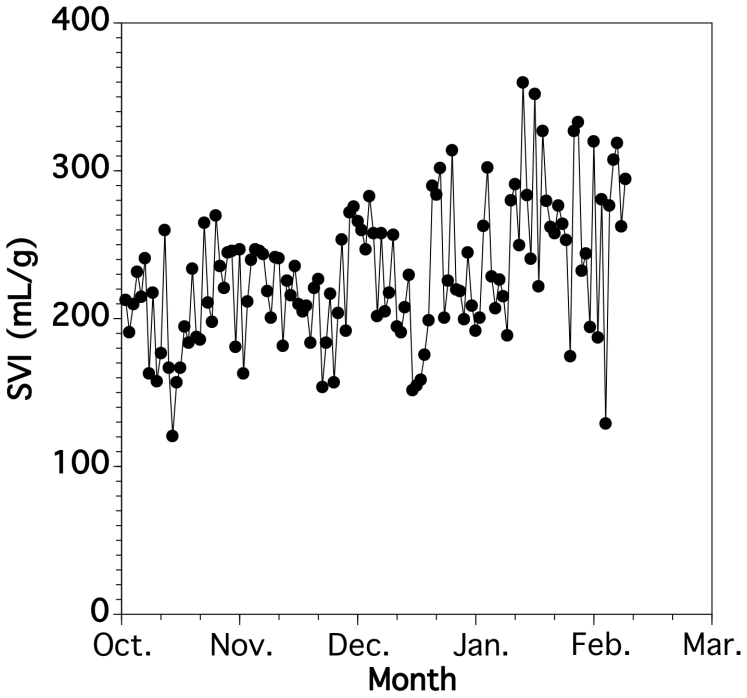

Figure S7. Time-course changes in SVI of AS of WWTP-M.

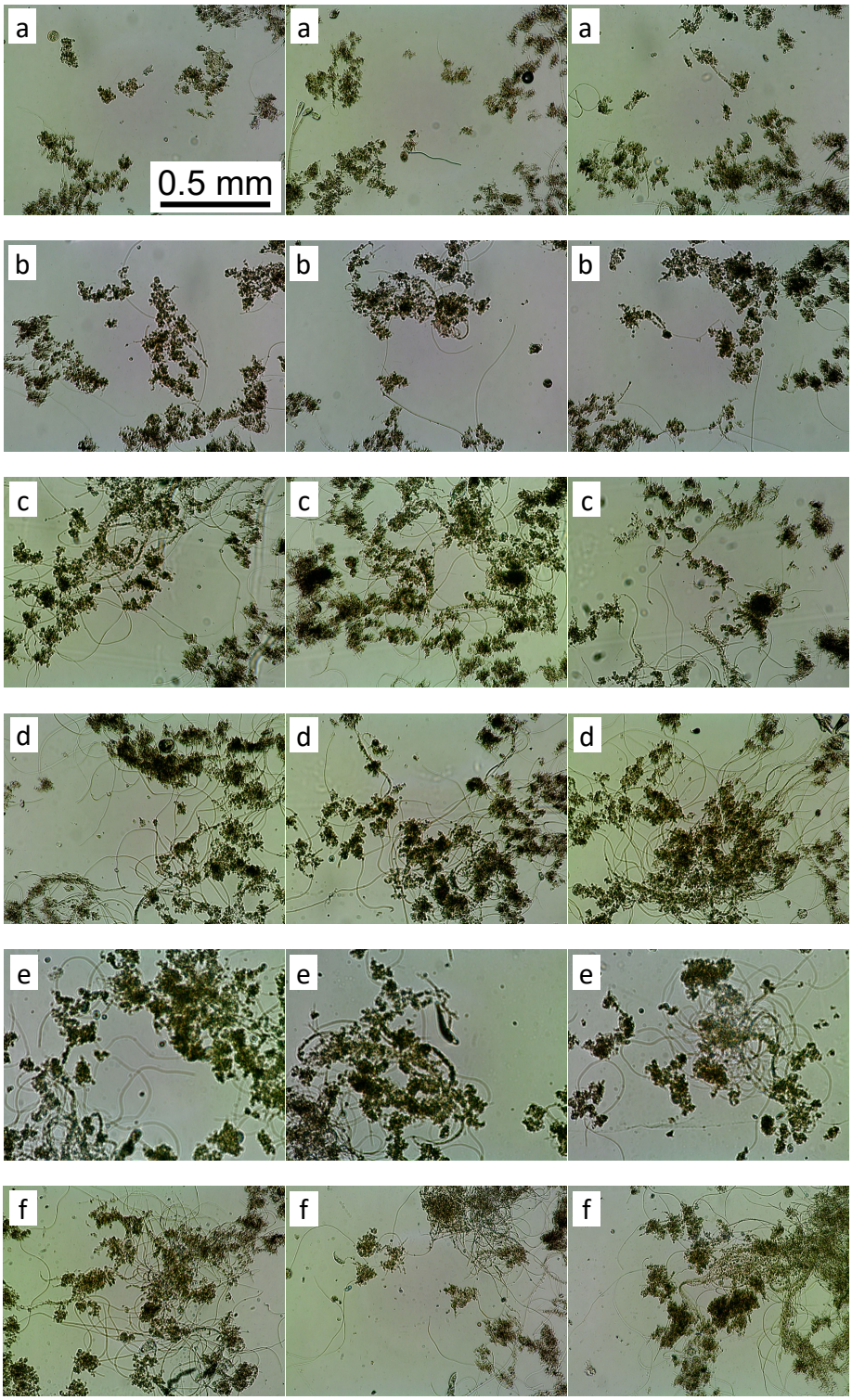

Figure S8. Typical microscopic images in bright field of AS flocs obtained from WWTP-M on (a) December 10th, (b) December 17th, (c) December 24th, (d) January 14th, (e) January 21st, and (f) January 28th.

489

490